A Fast Load Control System Based on Mobile Distribution-Level Phasor Measurement Unit

Wenxuan Yao, *Member, IEEE,* Shutang You, *Member, IEEE,* Weikang Wang, *Student Member, IEEE,* Xianda Deng, Yicheng Li, Lingwei Zhan, *Student Member, IEEE,* and Yilu Liu, *Fellow, IEEE*

***Abstract*— The increase of renewable penetration in power grids calls for loads to participate in frequency regulation to avoid under-frequency load shedding after large resource contingencies. The motivation of this paper is to fulfill a fast residential load control for frequency stability enhancement. For this purpose, a novel Mobile Distribution-level Phasor Measurement Unit (MDPMU) is developed for disturbance event detection, power mismatch estimation and fast load control. First, the systematic design of the MDPMU introduced. The proposed MDPMU has the major advantages of low cost and high frequency measurement accuracy. Second, the distribution-level measurement is utilized for the Rate Of Change Of Frequency (ROCOF) calculation. Upon detection of a power system frequency event, power mismatch is estimated at the early stage of the event. Details of a robust approach to calculate ROCOF and determine the event starting point are presented. Practical issues including the measurement reporting rate and estimation time are also considered. Last, with the proposed control system, residential load responses can be controlled coordinately based on load availability and compensation prices offered by customers, providing adaptive frequency regulation service after large resource contingencies. The accuracy of frequency measurement and power mismatch estimation are evaluated via experimental analysis. The frequency stability improvement by load control is validated via PSS/E simulation.**

***Index Terms*—Distribution-level phasor measurement, load control, mobile DPMU, ROCOF, power mismatch estimation**

I. Introduction

In the electric power industry, frequency stability is crucial to maintain stable power system operation since the fluctuation of frequency reflects the power mismatch between the generation and load demand [1][2]. Power unbalances can be caused by power system disturbances such as generation trip, tie-line trip or sudden change of loads. Every balancing authority is required to support the regulation of frequency, especially the recovery of system frequency after major disturbances such as a sudden generator trip [3].

The conventional frequency regulation solutions in the power industry are divided into three levels including Primary Frequency Regulation (PFR) [4], Secondary frequency regulation (SFR) [5] and Tertiary frequency regulation (TFR) [6]. However, recently increasing integration of renewable energy sources and nonlinear power electronic equipment bring about new challenges to the frequency stability in the following aspects: 1) The resource contingencies that introduce an instant mismatch between power generation and demand become more frequent and possibly larger in magnitude [7][8]. For example, the 2016 Blue Cut fire event caused 1.2 GW solar generation trip in California, U.S.[9] 2) Governor response has been decreasing due to displacement of synchronous generators with inverter-based resources that usually do not provide inertia and governor response, such as solar and wind generation.[10].

A. Background and Significance of Fast Load Control

Recently, as more and more residential loads become controllable, some responsive loads [11] with thermal storage features such as electric water heaters and air-conditioners, can be switched off for a short period to compensate the power mismatch to arrest frequency decline when the frequency drops below a threshold. Since water and air have a heat capacity, the temperature changes little in a short period. For example, based on the heat transfer model of electric water heater, water in typical heaters cool down 0.3°C per hour without hot water consumption and the heating element [12]. As a result, switching off such thermal storage feature responsive loads at the time scale of seconds hardly affects the comfort level of the residential customers. Ref. [13] studied using thermostatically controlled loads to control frequency, and found that estimating the states of thermostatically controlled loads can help reduce communication infrastructure with some sacrifice in accuracy. In general, besides thermostatically controlled loads, all other loads can participate in frequency regulation if incorporating load information appropriately. The information includes the cost of their switching on/off actions and consequent comfort reduction of customers, as well as their real-time availability for control. It is also noted that the amount of each individual load can be very small, but the effect can become significant considering the aggregated responses from many customers. In light of this, several frequency-based load control methods have been proposed [14]-[16] to coordinate the distributed load responses assuming load statuses are unknown or only partially known.

Manuscript received October 14, 2018; revised February. 21, 2019, and May 17, 2019, accepted June 26,2019. This work was supported in part by the Engineering Research Center Program of the National Science Foundation and the Department of Energy under NSF Award Number EEC-1041877, in part by the CURENT Industry Partnership Program and in part by U.S. Department of Energy (DOE) under the Grid Modernization Laboratory Consortium (GMLC) program. Paper no. TSG-01573-2018. *(Corresponding author: Wenxuan Yao)*

W. Yao and Y. Liu are with the Department of Electrical Engineering and Computer Science, University of Tennessee, Knoxville, TN, 37996, USA and also with Oak Ridge National Laboratory, Oak Ridge, TN, 37830, USA (email: wyao3@vols.utk.edu, liu@utk.edu)

S. You, W. Wang, X. Deng and Y. Li are with the Department of Electrical Engineering and Computer Science, the University of Tennessee, Knoxville, TN, 37996, USA. (e-mails: syou3@utk.edu, wwang72@vols.utk.edu, xdeng6@vols.utk.edu, yli137@vols.utk.edu,)

L Zhan is with Oak Ridge National Laboratory, Oak Ridge, TN, 37830, USA (email:zhanl@ornl.gov)

Different from existing studies, the load control system developed in this paper can make load statuses fully known at low costs and thus robust frequency regulation becomes possible. In addition, the power mismatch can be estimated before the frequency declines to the nadir so that frequency decline can be arrested timely after a contingency while avoiding frequency overshoot. For example, it is revealed in Ref. [17][18] that it takes up to 10 seconds for frequency dropping to a nadir during an actual Generation Trip Event (GTE) in U.S. Eastern Interconnection (EI). Considering that if the frequency can be measured at sufficiently high resolution and a fast control scheme is properly designed, the controller is able to take action to control residential loads coordinately and adaptively at the early stages of events, which will be helpful to avoid large frequency decline.

B. Related works on Distribution-level Phasor Measurement Unit

Several technical concerns exist in the practical implementation of fast load control. *First*, a high-resolution synchronized measurement device needs to be developed for large-scale installation at the distribution level. The cost should be affordable for regular households. Traditional monitoring devices such as Phasor Measurement Units (PMUs) were designed to install in substations at the transmission level, posing high manufacturing and installation costs. By utilizing Distribution-level PMU (DPMU) technology such as Frequency Disturbance Recorders (FDRs) in FNET/GridEye [19] and micro-PMUs (µPMUs)[20], monitoring costs have been greatly reduced. The Micro-PMU aims to monitor the distribution system in real time to improve its observability with high angle resolution [21]. However, the FDR and µPMU are still cost prohibitive for end-users. *Second*, current PMUs can only allow monitoring but lack data processing, power mismatch estimation, and control functions. They must send measurement data to a Phasor Data Concentrator (PDC) via the C37.118.2 protocol [22], which introduces time delay in data transmission and thus limits their applications in real-time control. *Third*, most existing model-based control schemes do not consider several practical issues such as the impact of calculation time and measurement noise on the control system.

C. Motivation

Following this, the motivation of this paper is to present a fast load control system at the residential level using DPMUs. The widely used mobile platform can achieve high computational performance to execute real-time measurement algorithms [23][24]. Taking advantages of this capability, the research team developed a Mobile DPMU (MDPMU) to perform fast phasor calculation. Using these synchronized frequency measurements in phasor data, power grid disturbance events can be real-time detected on the mobile platform. After an event is detected, a series of Rate of Change of Frequency (ROCOF) values is calculated to estimate the starting point of the event. Then power mismatch is estimated via ROCOF at an early stage of the event. The load availability and each customer's compensation price offer in providing frequency regulation service are considered to determine the control action of each load to a contingency. Measurement devices can communicate with smart breakers to achieve fast load control to improve frequency stability. The prototype of the whole system is built using EATON Energy Management Circuit Breaker (EMCB) [25] and an Android™-based mobile platform. It is noted that the whole design can be generalized to any advanced embedded systems and smart breakers.

Compared with previous work, the major advantages of proposed method include: 1) reduced costs and efforts for manufacturing, installation, and maintenance; 2) functions of real-time event detection and power mismatch estimation, which cannot be achieved by current DPMUs; 3) and the capability of communication with smart breakers for fast load control.

The rest of the paper is organized as follows. Section II introduces the development of MDPMU. The measurement accuracy is also evaluated via laboratory experiments. Section III presents the methodology for event detection and power mismatch estimation using measurement data. Section IV presents the fast load control method using estimated power mismatch, load availability and cost information from users. Simulation studies are also conducted for performance evaluation in this section. Finally, Section V concludes the paper and discusses future research directions.

II. Development of MDPMU

A. Hardware Design

At the hardware structure level, the MDPMU includes a Data Acquisition Board (DAQB) for a synchronized sampling of the distribution level power grid and a mobile unit for data

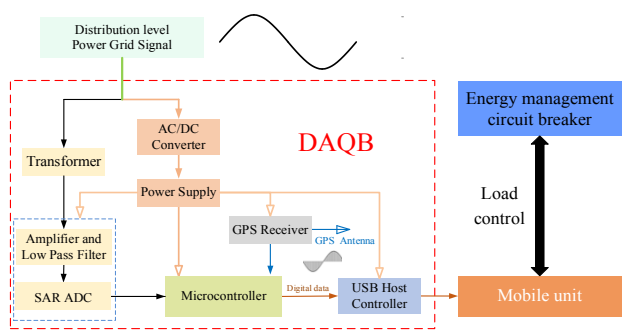

Fig. 1 Illustration of hardware struecture of mobile DPMUs

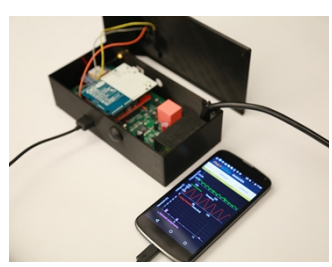

Fig. 2 Prototype of the MDPMU

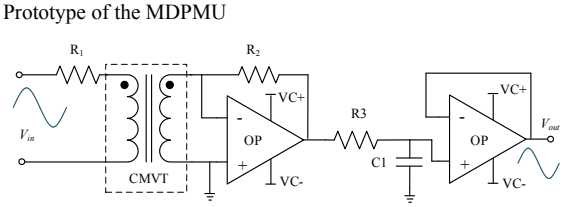

Fig. 3 Schematic design of input voltage channel

processing. The main reasons to choose mobile unit as a data processing center are: 1) high computational performance of current mobile platforms 2) built-in communication channel e.g., WIFI and 4G LTE, which is able to send commands to smart breakers for fast load control; 3) large capacity internal memory and the capability of caching measurement data for in-memory computation, 4) low costs and wide usage that will facilitate future deployment.

In the prototype development, an Android-based Nexus 4 equipped with a 16 GB memory and 1.5 GHz CPU clock is used as mobile unit. An Arduino board is used in DAQB to sample the analog signal and send the raw digital data to the mobile unit for data processing. Fig. 1 shows the systematic diagram. Fig.2 shows the prototype of MDPMU. An AC/DC converter combined with a voltage regulator provides power to the DAQB. Fig. 3 shows the circuit diagram of a voltage input channel for distribution grid signal acquisition. In this prototype, a Current-type Microminiature Voltage Transformer (CMVT) is used to scale down the voltage of power grid V_{in} to fit to the input range of Analog to Digital Converter (ADC). The frequency range of CMVT is 20Hz to 20 kHz and non-linearity error is below 0.1%. The magnitude of output voltage V_{out} can be expressed as

$$V_{out} = \mathrm{TR} \times V_{in} \times \frac{\mathrm{R_2}}{\mathrm{R_1}} \tag{1}$$

where TR is the turn ratio between the primary and secondary windings of CMVT. $\mathrm{R_3}$ and $\mathrm{C_1}$ form a low-pass anti-aliasing filter with a cutoff frequency $\frac{1}{2\pi \mathrm{R_3 C_1}}$. In the prototype, $\mathrm{R_1}$, $\mathrm{R_2}$ and TR are 67kΩ, 3 kΩ and 1, respectively. A successive approximation register type ADC (LTC1609) [26] is used to sample V_{in} at a 16-bit resolution and a 94.2-dB signal-to-noise ratio. The sampling interval and GPS-based synchronization is controlled by a microcontroller in DAQB. To avoid any data loss, two arrays work alternately in the microcontroller for receiving samples and sending samples to the mobile unit. The mobile unit communicates with DAQB via a Universal Serial Bus (USB) controller [27]. Upon receiving digital data, the mobile unit performs phasor calculation. Furthermore, the mobile unit achieves event detection and power mismatch estimation using real-time measurements. To realize load control, EMCBs with the Internet of Things (IoT) connectivity architecture [25] are used to receive commands from proposed mobile units and control on/off conditions of connected residential loads.

B. Software Design

1) Synchronized sampling on DAQB

The main task of DAQB is the synchronized sampling, which is the foundation for accurate frequency measurement. Since the precision of the 1 pulse-per-second (PPS) signal retrieved from a GPS receiver is in the nanosecond level and without accumulative errors [28], DAQB uses the 1PPS to discipline a sampling cycle. For other sampling intervals between two adjacent PPS signals, the sampling intervals are controlled by a timer in the microcontroller:

$$G = \frac{f_{osc}}{f_s} \tag{2}$$

where G is the number of clock pulses to count for each sampling period, f_{osc} is the clock speed, and f_s is the desired sampling rate. However, two challenges exist in actual implementation. First, due to changes in temperature and aging, the actual output frequency of the DAQB's onboard oscillator is likely to drift from its nominal value, which means that f_{osc} in (2) is not constant [29][30]. If f_{osc} is treated as a constant value, it would degrade the precision of sampling time control. Second, the Time Period Register (TPR) in any type of microcontroller has to be configured as an integer number while H is likely to be a fractional number according to (2). The integer restriction of TPR will introduce a division remainder and introduce sampling time error.

To compensate the sampling time error caused by the clock drifts of a commercial oscillator and division remainder of timer control, an adaptive sampling approach is adopted in the DAQB. First, to cope with f_{osc} drifting, real operating f_{osc} is measured using PPS as the reference. The clock pulses from the oscillator are counted between rising edges from M adjacent PPS signals. As illustrate in Fig.4, the rising edges of the PPS will be detected through an external interrupt in the microcontroller for Oscillator Frequency Measurement (OFM). The actual f_{osc} (denoted as f'_{osc}) can be obtained as

$$f'_{osc} = \frac{TP}{M} \tag{3}$$

where TP is total number of pulses counted within M consecutive PPS signals. Replacing f_{osc} by f'_{osc} in (2), the negative impact of f_{osc} drift can be eliminated. Second, to compensate the error caused by the integer restriction, a Two-value Variable Sampling Interval Control (TVIC) is adopted as illustrated in Fig. 4. Defining G_A and G_B as the nearest integers around G, satisfying $G_A + 1 = G_B$, G_A and G_B are alternately set as TPR to approach the actual fraction number G in (2). The criterion to the selection between G_A and G_B can be referred to Ref. [31]. The digital sampled packets are transmitted to the mobile unit via the USB interface.

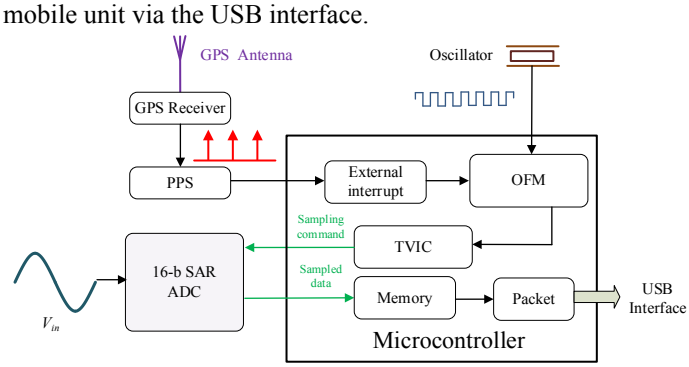

Fig. 4 Synchronized sampling in the microcontroller

2) Parameter calculation in mobile unit

On the MDPMU, an Application (APP) is developed based the Android operating system. The application consists of four major components including 1) USB communication component, 2) phasor calculation component, 3) event detection and power mismatch estimation component, and 4)

fast control component. It can run at Android 5.11 or higher version operation system.

After installing the application, the USB accessory connection status is continually monitored in the USB communication component. Once successful "handshake" is acknowledged between the DAQB and the mobile unit, the application in the mobile unit continuously receives data in its USB communication thread. Different from measuring signal on the high voltage level using conventional PMUs, the signal on distribution level has much worse power quality due to the harmonics and distortions produced by various electric appliances at the customer side [32]. Therefore, a recursive Discrete Fourier transform algorithm [33] [34] that immunes to harmonic distortion is used to achieve the accurate measurement in a noisy environment. After completion of each measurement in the calculation component, the measurement data set is used for fast event detection and power mismatch estimation, which will be discussed in details in Section III. When the amount of estimated power mismatch exceeds a certain threshold, whether a specific MDPMU responds to this event or not is determined by the event size and the optimal control scheme calculated by the load availability and user-input load control cost information. Through schemes looking up based on the event size, those responding MDPMU send commands to their connected smart breakers to execute the control component and achieve fast local control.

C. Measurement Accuracy evaluation

To evaluate the measurement accuracy of the MDPMU, experiments are conducted. The system setup is shown in Fig. 5. An OMICRON relay test platform (CMC 256) [35], equipped with CMIRIG B for GPS time synchronization, is used to generate simulated signals. For the test with signals in the distribution power grid, the measurements of the developed device are compared with measurements of an FDR for accuracy evaluation.

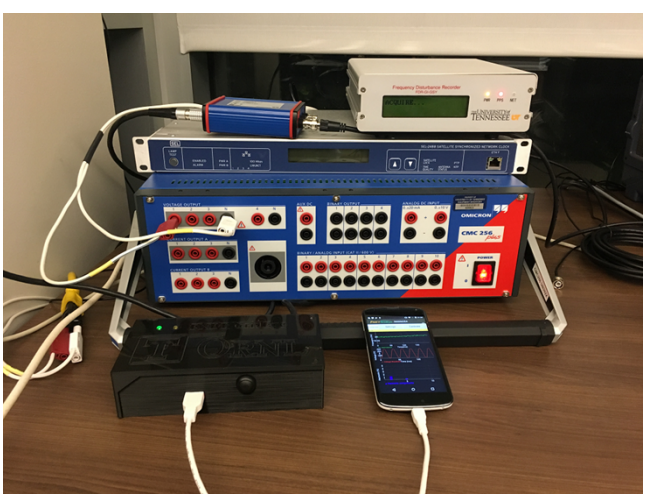

Fig.5. Experiment Setup

For the test using the OMICRON platform, the performance of the MDPMU is evaluated in different conditions: nominal/off-nominal frequency, harmonic distortion and dynamic states. To obtain statistical properties of results, the tests for each condition is conducted for at least 15 minutes. The nominal frequency is 60 Hz and excursion of $\pm 5 \times 10^{-2}$ Hz is selected for off-nominal frequency tests. For the harmonic distortion test, the 3rd order harmonic component with a 10% amplitude is added to the fundamental component. The modulation frequencies of 1 Hz and 2 Hz are considered respectively in testing phase modulation and amplitude modulation. The Maximum Absolute Error (MAE) and Root Mean Square Error (RMSE) of measurements over the simulated signal are listed in Table I. The RMSE under nominal, off-nominal and harmonic conditions are 5.25×10^{-4}Hz, 8.57×10^{-4}Hz , and 9.54×10^{-4}Hz, respectively, completely complying with IEEE standard C37.118 [36], which specifies that frequency error should be less than 5m Hz. For the dynamic compliance tests, the MAE is as small as 1.65×10^{-2} Hz, which is within the standard limit of 6.00×10^{-2} Hz in modulation conditions.

TABLE I. MEASUREMENT ERROR WITH SIGNAL FROM CMC 256

Test condition	Nominal	Harmonic	Off-nominal	
	60Hz	3rd order	59.95Hz	60.05Hz
MAE (Hz)	1.21×10^{-3}	1.78×10^{-3}	1.86×10^{-3}	2.01×10^{-3}
RMSE (Hz)	5.25×10^{-4}	8.57×10^{-4}	9.54×10^{-4}	8.03×10^{-4}
Test condition	**Phase modulation**		**Amplitude modulation**	
	1Hz	2Hz	1Hz	2Hz
MAE (Hz)	1.34×10^{-2}	1.65×10^{-2}	2.54×10^{-3}	4.82×10^{-3}
RMSE (Hz)	1.04×10^{-2}	1.29×10^{-2}	1.79×10^{-3}	2.95×10^{-3}

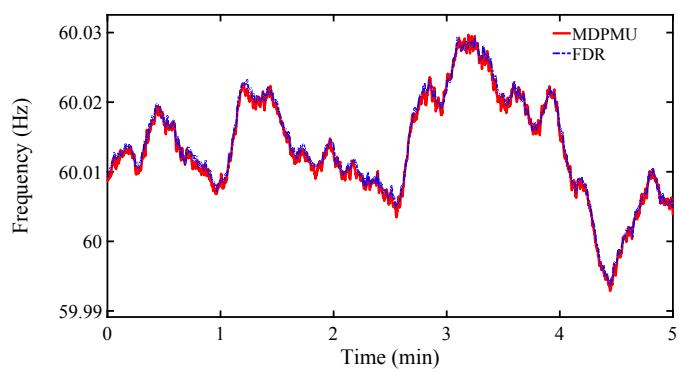

(a)

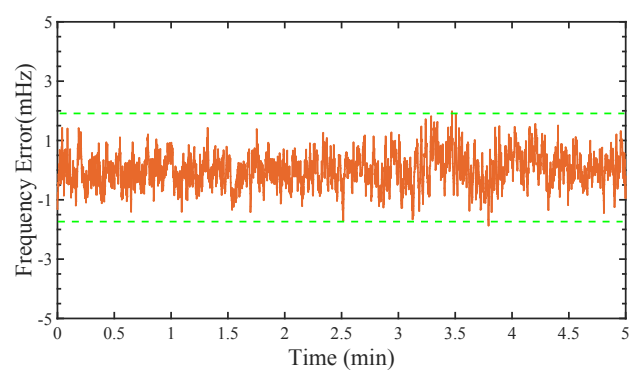

(b)

Fig. 6 Measurement results for signals from the distribution-level power grid (a) Raw frequency measurements for FDR and MDPMU (b) Error of MDPMU using FDR measurement as a reference

To further verify the effectiveness of the developed MDPMU, test using signals from distribution-level power grid is performed. Since the "true" frequency of the real world is unknown, an FDR [37] is set up to provide a reference for accuracy evaluation. The 5-minute continuous measurements are plotted in Fig. 6. It shows that MDPMU is capable to capture the trends over time. The differences between these two devices are posed by the hardware resolution limits, e.g., ADC and GPS timing random accuracy (1 microsecond). The error of MDPMU is below 1.8 mHz as shown in Fig.6(b), which is close to 1 mHz measurement resolution of FDR. It is noted that these errors will not accumulate with time. Thus in a large time window, the two measurements match quite well, verifying that the MDPMU can achieve the same accuracy level as that of an FDR for distribution level frequency monitoring.

III. Event Detection and Power Mismatch Estimation

A. Event Detection

Since the proposed mobile DPMU is capable of caching measurement data locally and performing in-memory computation, event detection can be achieved in real time. When the MDPMU obtains a dataset of measurements at a reporting rate R, an n point median filter is applied to remove isolated spikes and outliers in measurement data:

$$f^{i}_{median} = median(F^{i}) \tag{4}$$

where $F^{i} = \{f_{i+1}, f_{i+2}, \ldots, f_{i+n}\}$; i is the time index of the measurement dataset. Then the Frequency Change (FC) is calculated within a sliding window.

$$FC_i = \left| f^{i+R}_{median} - f^{i}_{median} \right| \tag{5}$$

AFC is defined as the accumulation of the FC over a certain time period, which is given by

$$AFC_i = \sum_{i=t_1}^{t_2} FC_i \tag{6}$$

where t_1 and $t_2$are the start and end time index, respectively, for this integration time period.

With these parameters introduced, the detection algorithm using the FC and AFC can be obtained in two phases. The flowchart of the event detection is shown in Fig. 7.

Phase I.

At time index i, FC_i is calculated via (5). Once FC_i surpasses threshold ε_1, an early event warning is initiated and the detection procedure goes to *Phase II:*

$$FC_i \geq \varepsilon_1 \tag{7}$$

Since the actual frequency keeps fluctuating all the time, the purpose of this step is to detect events over a certain magnitude. ε_1 is determined based on the statistical analysis of recent 10-year historical event data (more than 1000 events with confirmed information from utilities)[39]. It is noted that ε_1 varies in different systems due to their frequency response characteristics [40]. According to our statistical analysis, in U.S. EI 95% events greater than 400WM has FC larger than 0.0033 Hz/s.

Over a long period of time, the value of ε_1 should have been updated per the size of an interconnected power grid. With the increasing introduction of new generation source, such as nuclear, wind, solar, etc., the size of the power grid will grow. The adjustment can refer to the change footprint of the BAL-003-1 standard[41]. Overall the power grid evolves slowly. With the help more confirmed events, it is suggested to update ε_1 every 5 years when the statistical characteristic changes.

Phase II.

Once the detection procedure enters *Phase II*, the AFC_i will be calculated over time period t_1 and t_2. If AFC_i exceeds a certain threshold given by (8), it indicates that the frequency experiences an instable change for a certain period of time. Then it can be confirmed that a disturbance has occurred and it goes to the step of power mismatch estimation, which will be discussed in the next subsection. Otherwise the procedure returns to *Phase I*

$$AFC_i \geq \varepsilon_2 \tag{8}$$

It is noted that the determination basis of ε_2 is similar as ε_1 via analysis of historical event data.

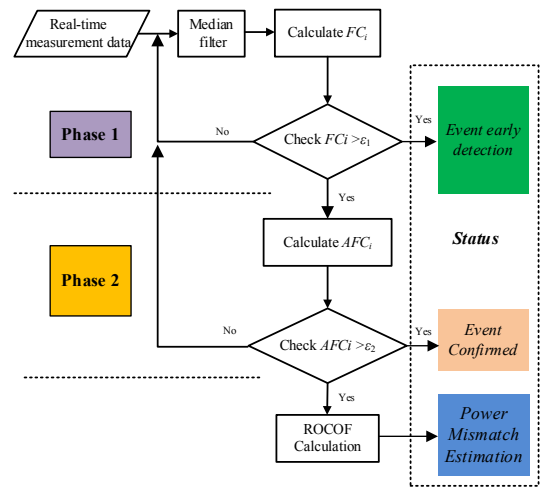

Fig. 7 Flowchart of the event detection module.

B. Power Mismatch Estimation

As shown in Fig. 7, the magnitude of power mismatch is estimated via the ROCOF calculation once an event disturbance is confirmed. According to Ref. [3], *ROCOF* reflects the power imbalance, which can be mathematically expressed as

$$ROCOF = \frac{\Delta P}{2H} \times f_0 + \frac{L}{2H} \times \Delta f \tag{10}$$

where L is the load damping and f_0 is the system frequency before the disturbance happens. H is the real-time system inertia, which depends on the online synchronous generators and synchronous motors. Control rooms can provide accurate H values based on real-time unit commit and load dispatch information. H can be made available to the public by system operators and updated every 15 minutes through Internet access of the MDPMU[38]. Δf is the system frequency deviation and ΔP is the generation-load mismatch of the disturbance relative to the system total MVA capacity.

Assuming the damping of load L is negligible, the power mismatch ΔP can be estimated as

$$\Delta P = ROCOF \times \frac{2H}{f_0} \tag{11}$$

It can be seen that ΔP is proportional to *ROCOF* and system inertia. As the system inertia is known, ΔP can be estimated via $ROCOF$.

Fig. 8 shows the comparison of frequency dynamics following three Generation Trip Events (GTEs) of different magnitudes in the EI. It can be seen that speed of frequency declines for large disturbances is higher than small events. Fig. 9 shows the relationship between ROCOF and the amount of power mismatch in the U.S. EI and Electric Reliability Council Of Texas (ERCOT) systems. It can be seen that the ROCOFs of both systems increase linearly with the power mismatch magnitude, which demonstrates the value of ROCOF can be used as an effective indicator to reflect power mismatch. The slope difference is mainly caused by different inertia between the two bulk systems.

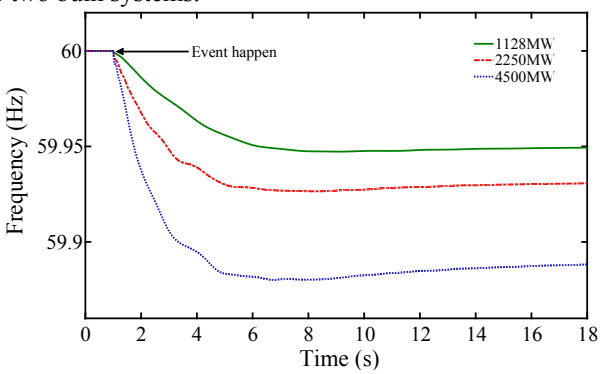

Fig. 8 Frequency dynamics of three generation trip events in EI

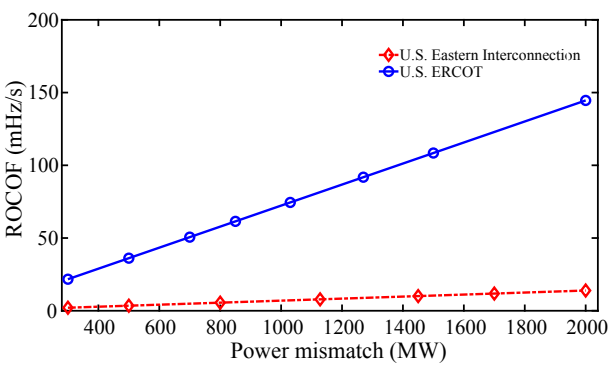

Fig. 9 Relationship between ROCOF and magnitude of power mismatch

C. *ROCOF calculation*

To improve the robustness of *ROCOF* calculation for actual measurements distorted by white noise, a least-square based polynomial curve fitting is applied. Defining time series measurements (t_i, f^i_{median}) with length *I*, a fitting polynomial $f_{median} = g(t_i)$ has the deviation error $\gamma_i = g(t_i) - f^i_{median}$ from each data point. The best fitting polynomial should satisfy

$$\min\|\gamma\|^2 = \min\sum_{i=0}^{I}\left(g(t_i) - f^i_{median}\right)^2 \tag{12}$$

The 2nd order polynomial $g(t_i)$ is expressed as

$$f^i_{median} = g(t_i) \approx \alpha_0 + \alpha_1 t_i + \alpha_2 {t_i}^2 \tag{13}$$

It is noted that 2nd order polynomial function is sufficient for capture the frequency trend at the initial stage of a disturbance.

Then, the polynomial function should also satisfy:

$$B = \min\sum_{i=0}^{I}\left(\sum_{j=0}^{2}\alpha_j t_i^j - f^i_{median}\right)^2 \tag{14}$$

where B is the sum of square of deviations. Taking the derivative of (14) and setting it to zero comes to the formula:

$$\frac{\partial B}{\partial \alpha_j} = 2\sum_{i=0}^{I}\left(\sum_{j=0}^{2}\alpha_j t_i^j - f^i_{median}\right)t_i^j = 0 \tag{15}$$

The coefficients α_j can be determined by a fixed equation in the form of (15). Thus the ROCOF can be calculated as

$$ROCOF = \frac{g(t_I) - g(t_0)}{t_I - t_0} \tag{16}$$

Substituting (16) into (11), power mismatch ΔP can be obtained within an *I*-second window. For GTEs, estimated ΔP of a disturbance can facilitate predicting the degree of frequency decline and improve the frequency nadir via the fast load control, and thus, significantly improve the overall system stability.

D. *Starting point determination*

Compared with a simulation study, it is more challenging to pinpoint the event starting point from measurements since the actual measurement data contains noise and local oscillation as illustrated in Fig. 10. By studying historical event data, we found that a sharpest jump always appears when an event begins. Making use of this characteristic, the starting point can be determined by searching the largest ROCOF. For the practical implementation, a series of ROCOFs with sliding windows is calculated when a disturbance is confirmed and then the local maximum of *ROCOF* is selected. Then the first point of its corresponding calculation window is regarded as the starting point. Fig. 11 shows continuous ROCOFs for two GTEs using sliding windows where maximum points can be pinpointed to determine the starting points.

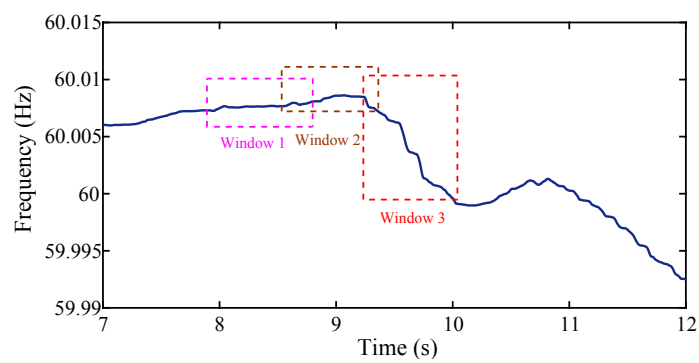

Fig. 10 Illustration of sliding windows for starting point determination

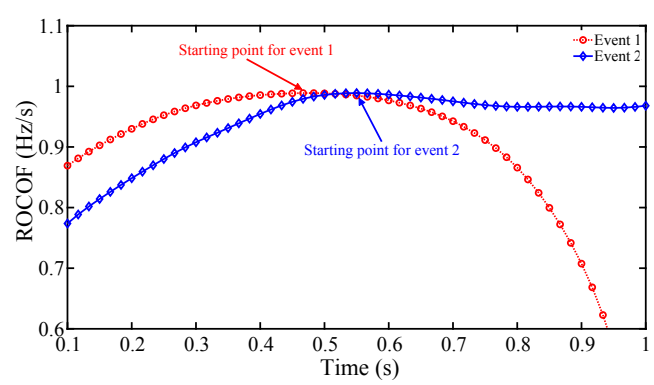

Fig. 11 Continuous ROCOFs of two GTEs

IV. Fast Load Control System and Performance Evaluation

In this section, the implementation of fast load-control system based on the MDPMU and EATON EMCBs is introduced as a prototype. In addition, the performance of power mismatch estimation is evaluated. Finally, the frequency behaviors with load control are studied via simulation.

A. *Load control system*

The load control system includes multiple MDPMUs installed at distribution level power grid to perform GPS synchronized monitoring and EMCBs to control the residential loads, as illustrate in Fig. 12. Communication between MDPMUs enables three important functions in load control: considering load availability, incorporating customers' willingness to participate in grid services, and coordinating multiple responsive loads to achieve the total amount of load response. More specifically, loads to response to this event is determined by:

$$\text{Minimize } C(x_{i,\Delta P_k}) = \sum_{i=1}^{N}\{c_i \cdot x_{i,\Delta P_k} \cdot s_i\} \tag{17.a}$$

$$\text{s.t. } \sum_{i=1}^{N}\{x_{i,\Delta P_k} \cdot p_i \cdot s_i\} \in [\Delta P_{k,min}, \Delta P_{k,max}] \tag{17.b}$$

where $x_{i,\Delta P_k}$ is the control action flag of load i when power mismatch is ΔP_k. c_i is the cost of load i for frequency response. It can be set by each customer based on willingness of providing grid service through sacrificing some potential comfort. s_i is the responsive load availability status of load i: 1 represents available and 0 is unavailable. p_i is the load response power of load i. $\Delta P_{k,min}$ and $\Delta P_{k,max}$ are the minimum and maximum values of the total load response power for an event with a ΔP_k magnitude. The results of this program is the distributed load control scheme $\{x_{i,\Delta P_k}\}$, which consists of load control action flags for different EMCB-controlled loads ($i \in [1,N]$) and event magnitudes ($\Delta P_k, k \in [1,K]$).

This mixed integer linear programming problem in (17) is calculated for a range of event magnitude ($\Delta P_k, k \in [1,K]$) and updated once it finds an update of the optimal solution due to change in the load availability or response costs. After power mismatch is estimated, the MDPMU sends control commands to EMCB according to the optimized control action flags based on a distributed load control scheme as illustrated in Fig. 12. The EMCB uses Google Firebase as its main server. After the database initialization, the mobile unit can directly send the command to EMCB via WIFI to control the connected residential loads. The status of the EMCB is real-time monitored by the MDPMU. If the latest control command fails to change the state, the MDPMU immediately re-issues another control command. In the prototype, we use the WIFI for convenience since the data transfer volume is not large. The measurement device only needs to receive on/off status of the smart breaker and send commands for load control. In the future, dedicated communication channels or direct connection between MDPMU and smart breakers can be utilized for security enhancement and time delay reduction

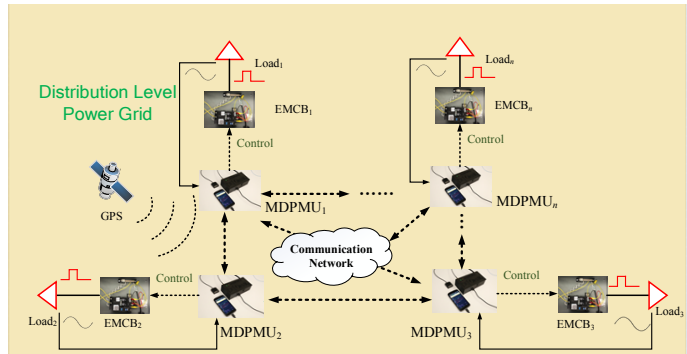

Fig. 12 Illustration of fast load control system in distribution level power grid

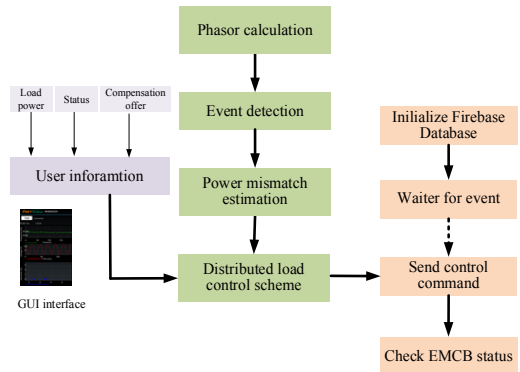

Fig. 13 Flowchart of load control system

B. *Real-time power mismatch estimation*

To evaluate the performance of power mismatch estimation, the average estimation error and time are calculated using historical large power system event data. The results are listed in Table II. For the test event dataset, the average power mismatch and event duration time are 811.51 MW and 11.57 s. From Table II, it can be seen that the case with higher reporting rate has smaller estimation time and error, which indicates that increasing reporting rate helps improve performance of the estimator. For the case of 120 Hz reporting rate, the relative power mismatch error is as small as 20% and the whole estimation process can be completed within 1.3 seconds while most of the events last more than 10 seconds. Therefore, such estimated magnitude of power mismatch is prompt and valuable information for the controller to take action for frequency regulation when a large frequency disturbance arrives.

TABLE II. Error and Time of Power Mismatch Estimation with Different Reporting Rates

Reporting Rate (Hz)	10	30	60	120
Estimation error (MW)	207.53	187.57	134.24	126.18
Estimation time (s)	1.9	1.5	1.4	1.3

C. *Simulation for fast load control in ERCOT*

The purpose of this subsection is to verify the effectiveness of fast load controls on frequency regulation using power mismatch estimation via simulation since it is not practical to implement the large-scale fast load control in field at current

stage. The simulation study is performed using the 6k-bus ERCOT model [42]. Case study of 2750MW (the largest resource contingency in [41]) GTE is performed in simulation. The controller and breaker are simulated using user-defined models in PSS/E. The communication of all MDPMUs is simulated using a python program to integrate into PSS/e simulation. The power mismatch estimation error and time listed in Table II are considered when applying the load control in simulation. The frequency behaviors with different reporting rate are shown in Fig. 14. It can be seen that the load reduction effectively offsets the generator power decrease by applying fast load control, therefore frequency drop and recovery time are significantly reduced. It is also demonstrated the high reporting rate with more accurate estimation magnitude and shorter estimation time can improve the performance of load control. To test the adaptiveness of the proposed distributed load control system, another GTE with 1664 MW generation loss is simulated and the result is shown in Fig. 15. The result indicates that the load control system can effectively adjust the load control scheme based on event magnitudes. With help of fast load control, frequency nadir does not drop to the Under Frequency Load Shedding (UFLS) for this large generation trip event. To investigate the impact of communication time on the performance of frequency response, simulations of above cases are carried out with additional time delay consideration. Fig. 16 shows the change of frequency nadir when communication time delay increases from 0 to 5 seconds. It can be seen that the frequency nadir changes almost linearly with the communication time delay. It shows that the communication time delay will result some error in load response because some loads' statuses may change during MDPMU communication.

It is noted that the whole control system is designed to take a prompt action under a disturbance, which requires a high-speed communication to coordinate multiple responsive loads. However, under certain circumstance, communication congestion or even failure may occur, which will result a large time delay and greatly degrade the performance of the control effect. Moreover, as listed in Table II, there is an average 126MW power mismatch estimation error for 120 Hz reporting rate, which is inevitably caused by the combined effects of measurement error, system inertia fluctuation [43], and system model simplification in Eq.(11). This error on power mismatch estimation will lead to the imperfection load control during large disturbance.

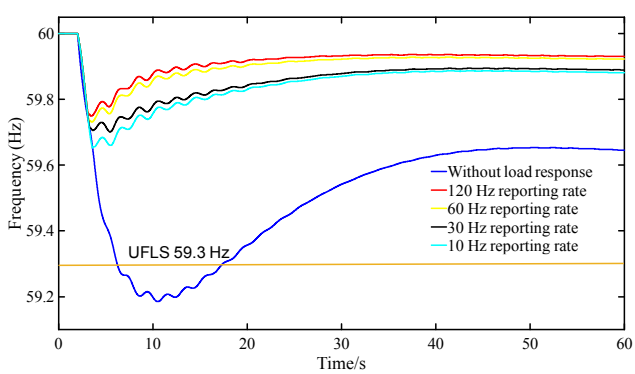

Fig. 14 Frequency response improvement with load control (2750MW generation loss)

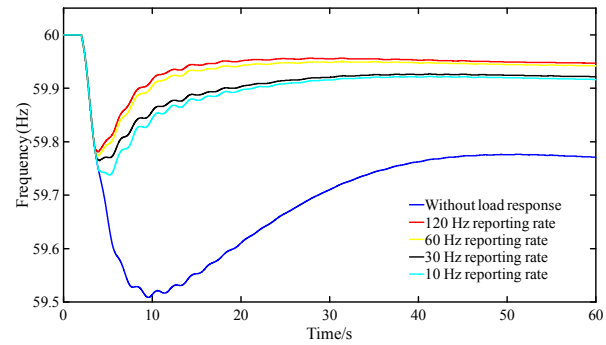

Fig. 15 Frequency response improvement with load control (1664 MW generation loss)

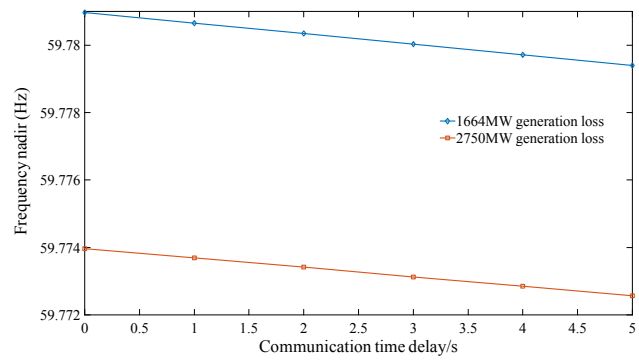

Fig. 16 Change of the frequency nadir with communication time delay

V. Conclusion

This paper presents a fast load control system that utilizes DPMU technology for event detection and power mismatch estimation. The main contribution can be highlighted as

1) A MDPMU is developed using GPS synchronization for the monitoring of electric energy systems. The cost of the proposed system is below 300 USD per unit, which is affordable for residential customers. A GPS-disciplined adaptive sampling strategy is adopted in data acquisition board. The performance of the developed prototype is evaluated via experiments.
2) Large power system disturbance can be detected in real-time via threshold criterion on frequency measurement. ROCOF values are calculated to determine the starting point of the event. Then power mismatch is estimated via ROCOF at an early stage of the event. Several practical issues including starting point determination, reporting rate and estimation time are considered. The simulation studies show the effectiveness of power mismatch estimation using measurements. Specifically, the power mismatch estimation method can achieve the 100 MW-level accuracy at the early-stage of event (1.3 seconds) with a 120 Hz reporting rate.
3) The MDPMU can communicate with smart breakers to achieve fast load control to improve frequency stability. The information obtained by MDPMU from distribution-level power grid makes it feasible for fast load response in the residential side. The residential load control availability, control compensation offering prices, and the event magnitudes are considered to achieve reliable, adaptive and economic frequency regulation. The prototype based on a

MDPMU and an EATON EMCB has been built as an implementation example of the proposed control system. The whole design can be generalized to any mobile embedded systems and smart breakers. Simulation on PSS/E is conduced to demonstrate the improvement of frequency stability via fast load control under large disturbance.

For the future work, the error and waiting time for power mismatch estimation has to be reduced with help of higher reporting rate (currently 120 Hz at highest) using advacned synchrophasor technologies. A full compliance tests mandated in C37.118 standard will be carried out before the commercialization. Furthermore, the coordination of distributed load control and field tests for demonstration of frequency reliability improvement via fast control are another directions to focus in the future.

REFERENCES

[1] Q. Shi, H. Cui and et al, "A hybrid dynamic demand control strategy for power system frequency regulation," *CSEE Journal of Power and Energy Systems*, vol. 3, no. 2, pp. 176-185, June 2017.

[2] R. Gardner and Y. Liu, "Generation-Load Mismatch Detection and Analysis," *IEEE Trans. Smart Grid*, vol. 3, no. 1, pp. 105-112, March 2012.

[3] H. Bevrani, Robust Power System Frequency Control. New York, U.S.: Springer, 2009, pp. 16–17.

[4] B. Wang, D. Liu, X. Shan, D. Su and Q. Zhang, "A detection method for response time of overall primary frequency regulation of power grid," *IEEE Conference on Energy Internet and Energy System Integration*, Beijing, 2017, pp. 1-6.

[5] Z. Shuai, W. Huang and et al, "A Maximum Power Loading Factor (MPLF) Control Strategy for Distributed Secondary Frequency Regulation of Islanded Microgrid," *IEEE Trans. Power Electronics*., early access, doi: 10.1109/TPEL.2018.2837125

[6] R. Salahshour, E. Mirmoradi and H. Ghasemi, "EVs participation in energy and reserve market considering primary and tertiary frequency regulation constraints," *Smart Grid Conference (SGC)*, Tehran, 2014, pp. 1-6.

[7] Y. Liu, S. You, J. Tan, Y. Zhang and Y. Liu, "Frequency Response Assessment and Enhancement of the U.S. Power Grids Toward Extra-High Photovoltaic Generation Penetrations—An Industry Perspective," *IEEE Trans. Power Systems*, vol. 33, no. 3, pp. 3438-3449, May 2018.

[8] S. You et al., "Comparative Assessment of Tactics to Improve Primary Frequency Response Without Curtailing Solar Output in High Photovoltaic Interconnection Grids," IEEE Trans. Sustainable Energy, vol. 10, no. 2, pp. 718-728, April 2019.

[9] North American Electric Reliability Corporation, 1,200 MW Fault Induced Solar Photovoltaic Resource Interruption Disturbance Report, June, 2017, available[online]: https://www.nerc.com/pa/rrm/ea/1200_MW_Fault_Induced_Solar_Photovoltaic_Resource_/1200_MW_Fault_Induced_Solar_Photovoltaic_Resource_Interruption_Final.pdf

[10] S. You et al., "Impact of High PV Penetration on the Inter-Area Oscillations in the U.S. Eastern Interconnection," *IEEE Access*, vol. 5, pp. 4361-4369, 2017.

[11] J. D. Kueck, A. F. Snyder, F. Li and I. B. Snyder, "Use of Responsive Load to Supply Ancillary Services in the Smart Grid: Challenges and Approach," *IEEE International Conference on Smart Grid Communications*, Gaithersburg, MD, 2010, pp. 507-512.

[12] Qingxin Shi, Fangxing Li, Qinran Hu, Zhiwei Wang,Dynamic demand control for system frequency regulation: Concept review, algorithm comparison, and future vision, *Electric Power Systems Research*, vo. 154, 2018,pp 75-87.

[13] Mathieu, J.L., Koch, S. and Callaway, D.S., 2013. State estimation and control of electric loads to manage real-time energy imbalance. *IEEE Trans. Power Systems*, *28*(1), pp.430-440.

[14] X. Shi, J. Yu, J. Cao and T. Yong, "Decentralised frequency-based control of a population of heterogeneous ACs without power oscillations," *IET Generation, Transmission & Distribution*, vol. 12, no. 10, pp. 2471-2479, 2018.

[15] C. Zhao, U. Topcu, N. Li and S. Low, "Design and Stability of Load-Side Primary Frequency Control in Power Systems," *IEEE Trans. Automatic Control*, vol. 59, no. 5, pp. 1177-1189, May 2014.

[16] M. R. Vedady Moghadam, R. T. B. Ma and R. Zhang, "Distributed Frequency Control in Smart Grids via Randomized Demand Response," *IEEE Trans. Smart Grid*, vol. 5, no. 6, pp. 2798-2809, Nov. 2014.

[17] FNET/Grideye website, http://fnetpublic.utk.edu/sample_events.html

[18] North American Electric Reliability Corporation, "2017 Frequency Response Annual Analysis", 2017, available[online]: https://www.nerc.com/comm/OC/BAL0031_Supporting_Documents_2017_DL/2017_FRAA_Final_20171113.pdf

[19] Y. Liu et al., "Wide-Area-Measurement System Development at the Distribution Level: An FNET/GridEye Example," *IEEE Trans. Power Delivery*, vol. 31, no. 2, pp. 721-731, April 2016.

[20] A. von Meier, E. Stewart, A. McEachern, M. Andersen and L. Mehrmanesh, "Precision Micro-Synchrophasors for Distribution Systems: A Summary of Applications," *IEEE Trans. Smart Grid*, vol. 8, no. 6, pp. 2926-2936, Nov. 2017.

[21] H. Mohsenian-Rad, E. Stewart and E. Cortez, "Distribution Synchrophasors: Pairing Big Data with Analytics to Create Actionable Information," IEEE Power and Energy Magazine, vol. 16, no. 3, pp. 26-34, May-June 2018.

[22] IEEE Standard for Synchrophasors for Power System, C37.118.2, IEEE Power System Relaying Committee of the Power Engineering Society, 2014.

[23] Y. Liu, W Yao, L. Zhan, H. Lu and Wei Gao, "Mobile electric field sensor based phasor measurement unit for monitoring an electric power grid", U.S. Patent. No. 10024897, 2018

[24] W. Yao, H. Lu, M. J. Till, W. Gao and Y. Liu, "Synchronized Wireless Measurement of High-Voltage Power System Frequency Using Mobile Embedded Systems," IEEE Tran. Industrial Electronics, vol. 65, no. 3, pp. 2775-2784, March 2018.

[25] EATON Energy Management Circuit Breaker, website: http://www.eaton.com/FTC/utilities/EMCB/index.htm, copyright EATON product

[26] Linear Technology Corporation, LTC 1609, datasheet: http://www.analog.com/media/en/technical-documentation/data-sheets/1609fa.pdf, Analog Device copyright product

[27] MAXIM Integrated (2007), "MAX3421E, USB peripheral/host controller with SPI interface," copyright Maxim Integrated Products.

[28] Fan, Z. Zhang, M. Trinkle, A. D. Dimitrovski, J. B. Song and H. Li, "A Cross-Layer Defense Mechanism Against GPS Spoofing Attacks on PMUs in Smart Grids," *IEEE Trans. Smart Grid*, vol. 6, no. 6, pp. 2659-2668, Nov. 2015.

[29] F.L Walls and J. Gagnepain, "Environmental sensitivities of quartz oscillators," *IEEE Trans. Ultrasonics, Ferroelectrics, and Frequency Control*, vol.39, no.2, pp.241-249, March 1992

[30] F.L Walls and John R Vig. "Fundamental limits on the frequency stabilities of crystal oscillators," *IEEE Trans. Ultrasonics, Ferroelectrics, and Frequency Control*, vol.42, no.4, pp.576-589, July 1995

[31] W. Yao et al., "A Novel Method for Phasor Measurement Unit Sampling Time Error Compensation," *IEEE Trans. Smart Grid*, vol. 9, no. 2, pp. 1063-1072, March 2018.

[32] H. Wen and et al, "Power System Frequency Estimation of Sine-wave Corrupted With Noise By Windowed Three-point Interpolated DFT," *IEEE Trans. Smart Grid*, vol.9 no. 5, pp. 5163-5172 Sept. 2018

[33] J. Chen, "Accurate frequency estimation with phasor angles," M.Sc.thesis, Bradley Dept. Elect. Comput. Eng., Virginia Polytechnic Inst. State Univ., Blacksburg, VA, 1994.

[34] T. Xia, and Y. Liu, "Single-phase phase angle m copyright Maxim Integrated Products measurements in electric power systems," *IEEE Trans. Power System,* vol. 25, no. 2, pp. 844-852, May 2010.

[35] OMICRON, CMC 256 precision relay test platform, https://www.omicronenergy.com/en/products/cmc-256plus/

[36] IEEE Standard for Synchrophasors for Power System, C37.118.1, IEEE Power System Relaying Committee of the Power Engineering Society, 2014.

[37] Y. Liu et al., "A Distribution Level Wide Area Monitoring System for the Electric Power Grid–FNET/GridEye," *IEEE Access*, vol. 5, pp. 2329-2338, 2017.

[38] P. Du and J. Matevosyan, "Forecast System Inertia Condition and Its Impact to Integrate More Renewables," *IEEE Trans. Smart Grid*, vol. 9, no. 2, pp. 1531-1533, March 2018.

[39] D. Zhou, Y. Liu and J. Dong, "Frequency-based real-time line trip detection and alarm trigger development," I*EEE PES General Meeting Conference & Exposition*, National Harbor, MD, 2014, pp. 1-5

[40] Y. Ye, J. Dong and Y. Liu, "Analysis of power system disturbances based on distribution-level phasor measurements," *IEEE Power and Energy Society General Meeting*, San Diego, CA, 2011, pp. 1-7

[41] NERC, Standard BAL-003-1 — Frequency Response and Frequency Bias Setting, 2007, updated in 2015

[42] Electric Reliability Council of Texas, "2015 State of the grid," 2015, Available:[online]: http://www.ercot.com/content/news/presentations/2016/2015_StateoftheGridReport.pdf

[43] S. You and et al., "Non-Invasive Identification of Inertia Distribution Change in High Renewable Systems Using Distribution Level PMU," IEEE Trans. Power Systems, vol. 33, no. 1, pp. 1110-1112, Jan. 2018.

BIOGRAPHY

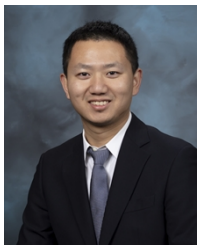

Wenxuan Yao (M'19) received his B.S. and Ph.D. degrees from the College of Electrical and Information Engineering, Hunan University, Changsha, China, in 2011 and 2017, respectively and the Ph.D. degree from Department of Electrical Engineering and Computer Science, University of Tennessee, Knoxville, USA, in 2018. He is currently a research associate in Oak Ridge National Laboratory. His research interests include wide-area power system monitoring, synchrophasor measurement application, embedded system development, power quality diagnosis and big data analysis in power systems.

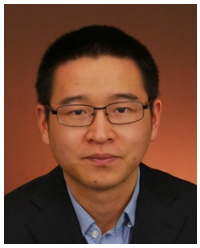

Shutang You (S'13–M'18) received the B.S. and M.S. degrees in Electrical Engineering at Xi'an Jiaotong University in 2011 and in 2014, and the Ph.D. degree in Electrical Engineering at the University of Tennessee, Knoxville in 2017. He is currently a research assistant professor in the Department of Electrical Engineering and Computer Science at the University of Tennessee, Knoxville. His research interest is in power grid dynamics and monitoring.

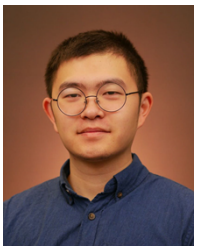

Weikang Wang (S'13) received his B.S. degree in Computer Science at the North China Electric Power University in 2016. He is currently a PhD candidate in Computer Engineering at the University of Tennessee, Knoxville. His research interest includes wide area monitoring, situation awareness, bid data, and machine learning.

Xianda Deng received his B.S. degree in electrical engineering, Guangxi University, Nanning, China in 2005, M.S. degree in electrical engineering from Arizona State University, Tempe, AZ, USA, in 2012. He is currently pursuing the Ph.D. degree in electrical engineering at University of Tennessee, Knoxville, TN, USA. From 2014 to 2016, he was an engineer in Midcontinent Independent System Operator, Carmel, IN, USA. His research interests include PMU related applications and data analysis.

Yicheng Li received the B.S. in computer science from the University of Tennessee, Knoxville in 2018. He currently is working towards his Ph.D. degree in the Department of Electrical Engineering and Computer Science, University of Tennessee, Knoxville, TN, USA. His research interest includes Message Passing Interface (MPI) derived datatypes and embedded mobile systems.

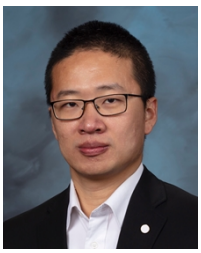

Lingwei Zhan (M'15) received the B.S. and M.S. degrees in electrical engineering from Tongji University in 2008 and 2011, respectively. He received his Ph.D. degree in the Department of Electrical Engineering and Computer Science at the University of Tennessee, Knoxville, in 2015. He is currently a R&D staff with Oak Ridge National Laboratory. His research interests include advanced grid sensors, PMU, synchrophasor measurement algorithm, wide-area power system monitoring, renewable energy sources, FACTs, and HVDC.

Yilu Liu (F'04) received her M.S. and Ph.D. degrees from the Ohio State University, Columbus, in 1986 and 1989. She received the B.S. degree from Xian Jiaotong University, China.

Dr. Liu is currently the Governor's Chair at the University of Tennessee, Knoxville and Oak Ridge National Laboratory (ORNL). Dr. Liu is elected as the member of National Academy of Engineering in 2016. She is also the deputy Director of the DOE/NSF-cofunded engineering research center CURENT. Prior to joining UTK/ORNL, she was a Professor at Virginia Tech. She led the effort to create the North American power grid Frequency Monitoring Network (FNET) at Virginia Tech, which is now operated at UTK and ORNL as GridEye. Her current research interests include power system wide-area monitoring and control, large interconnection-level dynamic simulations, electromagnetic transient analysis, and power transformer modeling and diagnosis.